Design, processing, and characterization of an optical core-bioactive clad phosphate fiber for biomedical applications

Availability:
This version is available at: 11583/2751804 since: 2023-04-20T08:10:58Z

Publisher:
Blackwell Publishing Inc.

Published
DOI:10.1111/jace.16553

Terms of use:

Publisher copyright

(Article begins on next page)

15 May 2024

Design, processing and characterization of an optical core - bioactive clad phosphate fiber for biomedical applications

Pablo Lopez-Iscoa[a], Nirajan Ojha[b], Diego Pugliese[a], Ayush Mishra[c], Regina Gumenyuk[b], Nadia Giovanna Boetti[d], Davide Janner[a], Johann Troles[e], Bruno Bureau[e], Catherine Boussard-Plédel[e], Jonathan Massera[c], Daniel Milanese[a,f,^] and Laeticia Petit[b*]

[a]*Politecnico di Torino, Dipartimento di Scienza Applicata e Tecnologia and INSTM research unit, Corso Duca degli Abruzzi 24, 10129 Torino, Italy*

[b]*Photonics Laboratory, Tampere University, Korkeakoulunkatu 3, FI-33720 Tampere, Finland*

[c]*Faculty of Medicine and Health Technology, Tampere University, Korkeakoulunkatu 10, FI-33720 Tampere, Finland*

[d]*Fondazione LINKS – Leading Innovation & Knowledge for Society, Via P. C. Boggio 61, 10138 Torino, Italy*

[e] *University of Rennes, CNRS, ISCR-UMR 6226, F-35000 Rennes, France*

[f]*IFN - CNR, CSMFO Laboratory, Via alla Cascata 56/C, 38123 Povo (TN), Italy*

^ *now at Department of Engineering and Architecture and RU INSTM, University of Parma, Parco Area delle Scienze 181/A, I-43124 Parma, Italy*

* Corresponding author: laeticia.petit@tuni.fi

Abstract

The aim of this study was to fabricate a bioactive optical fiber able to monitor "in situ" its reaction with the body through changes in its optical properties. Core and clad preforms were prepared with the composition $(97.25*(0.50P_2O_5-0.40SrO-0.10Na_2O)-2.5ZnO-0.25Er_2O_3)$ and $(98.25*(0.50P_2O_5-0.40SrO-0.10Na_2O)-1.75ZnO)$ (in mol%), respectively, and successfully drawn into a multi-mode core/clad optical fiber. Optical and near-Infrared images assessed the proper light guiding properties of the fiber. The fibers favor the precipitation of a Ca-P reactive layer at its surface concomitant with a reduction in the fiber

diameter, when immersed in SBF, often assigned as a sign of bioactivity. It is clearly shown here that the bio-response of the fiber upon immersion in SBF can be tracked from the decrease in the intensity of the Er^{3+} ions emission at 1.5 μm. This confirms that the newly developed optical fiber, which combines good optical properties with a suitable bioactive behavior, is a promising platform for the development of novel biomedical devices for biophotonic and photomedical applications. Finally, the successful splicing of the newly developed fiber with commercial optical fibers was an evidence of the possibility to integrate the phosphate fiber within existing components used in the field of biomedicine.

Keywords: phosphate glass, optical fiber, Er luminescence property, bioactivity

1. Introduction

Since the discovery of the first bioactive glass by Larry Hench in 1971 [1], several types of glasses, such as silicates and phosphates, have attracted the attention of many researchers, especially for biomedical applications [2–6]. Above all, phosphate glasses with a P_2O_5 content of around 50 mol% have been shown to be biocompatible [7–10], and the addition of other elements such as strontium was found to enhance the attachment, and proliferation of human gingival fibroblasts [12]. Moreover, the dissolution of phosphate glasses can be adjusted from hours to years depending on their composition and structure [13,14]. Thus, phosphate glasses have been studied in various biomedical applications, especially for use in bone repair and reconstruction [15].

Apart from their biological properties, phosphate glasses are also of great interest due to their easy processing, excellent thermo-mechanical and chemical properties, homogeneity, good thermal stability and excellent optical properties, such as high transparency in the UV-Visible-Near Infrared (UV-Vis-NIR) region [16–20]. Besides, phosphate glasses allow high

rare-earth (RE) ions solubility. Thus, concentration quenching phenomena do only occur at very high concentrations of RE [20,21]. In addition, phosphate glasses with P_2O_5 higher than 45 mol% have proven to be easily drawable into optical fibers [9,22–26]. Therefore, phosphate glasses have recently become appealing for the engineering of photonic devices for optical communications [27], laser sources and optical amplifiers [14,20,21,28,29]. However, to the best of our knowledge, only few studies focusing on glass compositions that combine both biocompatibility and suitable optical properties have been reported up to now [24,30].

Recently, optical fibers have gained a lot of interest for use in biomedical applications such as phototherapy, optogenetics, biological sensing and imaging [31]. Noticeable research efforts are spent in the development of biodegradable or bioactive optical fibers, which can be resorbed or can lead to new soft tissue once the therapeutic or sensing utility has been accomplished so that the surgical removal of the fiber sensor is not needed. In order to check the solubility and bioactivity, the glasses are typically immersed in tris buffer solution, phosphate buffered saline solution, simulated body fluid (SBF) or cell culture media.

In 2014, Massera *et al.* proposed the idea of tracking the bio-response of a glass fiber "in vivo" [32]. In this work, a bioactive phosphate fiber sensor with a molar composition of $50P_2O_5$-$40CaO$-$10Na_2O$ able to monitor its degradation and bio-response was reported. Part of the fiber was immersed in SBF and tris(hydroxymethyl) aminomethane (TRIS) solutions. Thereafter, the *in vitro* reactivity and the optical properties of the fiber were measured as a function of the immersion time. At the beginning, no change in the light transmission was reported. Then, there was a slow decrease in the light transmission due to the appearance of some calcium phosphate reactive layer, assumed to be a dicalcium phosphate dehydrate, forming at the surface of the fiber. For longer immersion times, the scattering of the reactive layer triggered a fast decay of light transmission. In the final stage, a thick reactive layer blocked the further degradation of the fiber.

In our previous study reported in [33], Er^{3+}-doped phosphate glasses within the glass composition of Na_2O-P_2O_5-SrO were developed with different compositions in order to understand the impact of the addition of Al_2O_3, TiO_2 or ZnO on the thermal, structural and luminescence properties of the glasses. The addition of Al_2O_3 and TiO_2 leads to a more connected the phosphate network, whereas the addition of ZnO does not modify the thermal and structural properties but leads to the increase of the emission intensity at 1.5 μm, thus indicating that ZnO-containing phosphate glasses are promising materials for laser applications.

In this paper, the feasibility to draw ZnO-containing glass into a fiber is shown. A multi-mode core/cladding optical fiber was fabricated with core and cladding glass compositions of $97.25*(0.50P_2O_5$-$0.40SrO$-$0.10Na_2O)$-$2.5ZnO$-$0.25Er_2O_3$ (in mol%) and $98.25*(0.50P_2O_5$-$0.40SrO$-$0.10Na_2O)$ -$1.75ZnO$ (in mol%), respectively. First, the motivation for selecting the above mentioned core and cladding glass compositions is addressed. One should mention that the concentration of the Er_2O_3 in the fiber is 0.25 mol%. After complete dissolution of the fiber in the body, the amount of Er_2O_3 in the body would be lower than 5000 mg/kg of body weight, the concentration that leads to acute toxicity in rat according to the Material Safety Data Sheet (MSDS) of Er_2O_3. Furthermore, SiO_2-CaF_2 glass-ceramic nanoparticles did not present signs of cytotoxicity althought they were doped with 1 mol% of Er_2O_3[34]. Then, the evaluation of the bio-response of the fiber using SBF as the medium is presented. Additionally, the changes in the fiber diameter and the transmission emission properties are investigated as a function of the immersion time in different aqueous solutions. Finally, the splicing of the active optical fiber with a commercial silica fiber and the resulting insertion loss is reported.

2. Materials and methods

2.1 Preform preparation and fiber drawing

A multi-mode core/cladding optical fiber with a core composition of $97.25*(0.50P_2O_5-0.40SrO-0.10Na_2O)-2.5ZnO-0.25Er_2O_3$ and a cladding composition of $98.25*(0.50P_2O_5-0.40SrO-0.10Na_2O)-1.75ZnO$ was successfully drawn. The core and cladding glasses were fabricated by melting a powder batch of 80 g in a quartz crucible at 1200 °C for 1 h, with a heating ramp of 5 °C/min. A further annealing at around their glass transition temperature (T_g) for 5 h was performed to release the residual stresses inside the glasses. In order to minimize the water content, the precursors were weighed and mixed in a glove box with a relative humidity < 0.1%. The core rod was prepared by the conventional casting method, while the cladding tube was obtained by rotational casting. The latter was performed by casting the cladding melt into a cylindrical mold preheated at 350 °C, which was subsequently put in rotation at a speed around 3000 rpm for few seconds. After annealing, the external surface of the core rod and cladding tube were optically polished. The diameter and the length of the core preform were 10.5 and 93 mm, respectively. Similarly, the length of the cladding was 82 mm, and the internal and outer diameters were 5.75 and 11.45 mm, respectively.

Prior to drawing, the core-cladding preform was obtained by the rod-in-tube technique inserting the stretched core (diameter 4.3 mm) into the cladding tube. The diameter and the length of the core/cladding preform were 11.45 and 80 mm, respectively.

The resulting core-clad preform was drawn by using the rod-in-tube method in a specially designed two meters high drawing tower as described in [30]. A schematic of the drawing tower can be found in [35]. To reduce the moisture concentration, the system was purged with Ar gas laminar flow at the rate of 3 l/min before the drawing. The thermal gradient of the drawing furnace permits to soften the preform just above its lower extremity. To avoid either nucleation or crystallization during the drawing, the temperatures of the hot-

zone and pre-heat zone were precisely mapped and the dwell time in these zones was controlled before and during the drawing. A narrow (5 mm-long) drawing furnace was used to decrease the time of presence of the glass in the critical high-temperature zone. The preform was drawn at 580 °C under helium gas laminar flow with rate of 2.5 l/min to create an inert controlled atmosphere around the preform. The fiber was drawn at a rate of ~3 m/min with a feed rate of 0.4 mm/min. A slight depression (-50 mbar) was applied between the core cane and the clad tube, in order to well collapse the two glass compositions. An uncoated fiber (without any protective polymer layer) was drawn to allow the measurement of the thermal, structural and optical properties. 40 meters of multi-mode core/cladding fiber with inner/outer diameters of around 50/120 µm were obtained.

2.2 Characterization

Differential Scanning Calorimetry (DSC): The glass transition (T_g) and crystallization temperatures were measured by using a Netzsch JUPITER F1 instrument. The measurement was carried out in a Pt crucible at a heating rate of 10 °C/min. T_g was determined as the inflection point of the endotherm obtained by taking the first derivative of the DSC curve, while T_x and T_p were taken at the onset and at the maximum of the exothermic peak, respectively. All measurements were performed with an error of ± 3 °C.

Optical microscopy: An optical microscope (Nikon Eclipse 50i) connected to a computer with a picture acquisition system was used to measure the fiber dimensions. The estimated error of the diameter measurement was ± 2 µm.

Elemental Dispersive Spectroscopy / Scanning Electron Microscopy (EDS/SEM): The fiber was examined by a scanning electron microscope (Carl Zeiss Crossbeam 540). The semi-quantitative elemental analysis of its composition was performed by using the Oxford Instruments X-MaxN 80 EDS detector within the accuracy of the measurement (±1.5 mol%).

Micro-Raman spectroscopy: The Raman spectra were acquired with a Renishaw inVia Reflex micro-Raman spectrophotometer (Renishaw plc, Wotton-under-Edge, UK) equipped with a cooled charge-coupled device (CCD) camera using a 785 nm excitation line. The spectra were recorded in the range 600–1400 cm^{-1} and were normalized at the maximum point (~1170 cm^{-1}).

Refractive index measurement: The refractive index (*n*) of the core and cladding glasses was measured at 633, 825, 1061, 1312 and 1533 nm by the prism coupling technique using a Metricon, model 2010. Ten scans were performed for each wavelength. The estimated error of the measurement was ± 0.001. The samples were 1 mm-thick optically polished disks. The refractive index experimental data were fitted using Sellmeier's equation [36]:

$$n^2(\lambda) = 1 + \frac{B_1 \cdot \lambda^2}{\lambda^2 - C_1} + \frac{B_2 \cdot \lambda^2}{\lambda^2 - C_2} + \frac{B_3 \cdot \lambda^2}{\lambda^2 - C_3} \qquad (1),$$

where λ is the wavelength and $B_{1,2,3}$ and $C_{1,2,3}$ are the experimentally determined Sellmeier's coefficients.

Near-field imaging: The near-field imaging was used to evaluate the guiding properties of the optical fiber. A laser light at 1300 nm with no interaction with the Er^{3+} ions was chosen as the lighting source. The investigated optical fiber was coupled to the laser diode source at 1300 nm and the output facet was observed with a CCD camera with magnifying lens.

Optical loss by cut-back method: The cut-back method was employed to assess the optical fiber losses. The optical loss (dB/m) was calculated using the following equation:

$$\alpha = 10 \; \frac{\text{Log}\left(\frac{P_{out}}{P_{out2}}\right)}{L - l} \qquad (2),$$

where P_{out} is the power output of a fiber with length *L*, and P_{out2} is the output power of the fiber with length *l*.

The measurements were taken before and after several sections of the fiber had been removed. The experimental data were fitted with a linear least square fitting. The slope of the

graph corresponds to the loss of the optical fiber, expressed in dB/m. The estimated error of the measurement was ± 10%.

The optical loss of the fiber was assessed using a 115 cm-long section butt-coupled with a single-mode silica fiber pigtailed laser diode source at 1300 nm (Infineon SBM 52414x). A Thorlabs PM100 equipped with S144A InGaAs power meter was used as a detector.

Bioactive response of the fiber in SBF: The SBF solution was prepared by following the methodology reported in the standard ISO/FDIS 23317 [37]. The fibers were first placed in a mold and then immersed in 3 ml SBF solution for up to 4 weeks at room temperature and also in a static incubator (Termaks, Norway) maintained at 37 °C. A schematic representation of the set-up is shown in Fig. 1.
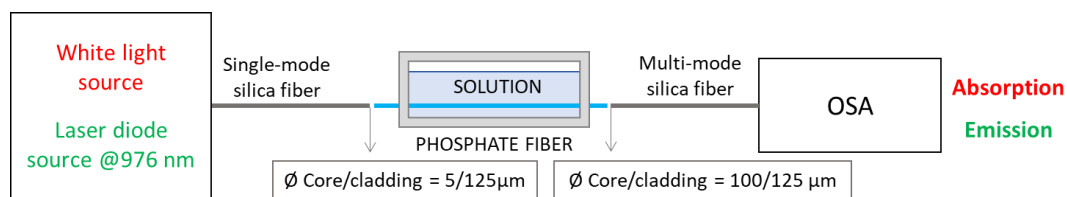

Fig. 1. Schematic representation of the set-up used for the absorption and emission measurements of the fiber immersed in different aqueous solutions.

The optical fiber with a length of 5 cm was butt-coupled to the light source and the power meter using two silica fibers. The transmission spectra of the fiber and emission spectra of the $Er^{3+}:^4I_{13/2}$ energy level in the range from 1400 to 1700 nm were collected at room temperature. The emission spectra were obtained by exciting the optical fiber with a fiber pigtailed laser diode operating at 976 nm (CM962UF76P-10R, Oclaro). The emission was recorded using a light power meter (PM100D from Thorlabs) and an optical spectrum analyzer (OSA) (Ando AQ6317B). The optical transmission through the phosphate fiber was

evaluated by using a broadband white light source (Thorlabs SLS201L) and the above mentioned OSA.

Splicing and insertion losses: The phosphate optical fiber was cleaved and fusion spliced with a commercial single-mode silica fiber (7/125 μm) by using the cleaver Fujikura CT-106 and the splicer Fujikura FSM-100P, respectively. Various trials with segments of around 10 cm of phosphate and silica fibers were spliced. Their insertion losses were obtained by measuring the difference in voltage between the input and the output power.

3. Results and Discussion

In order to manufacture a high quality optical fiber, the glasses used as the core and the cladding need to possess specific properties. At first, the glasses should be mechanically resistant upon casting and also stable against crystallization, i.e. the difference between their onset of crystallization temperature, T_x, and their glass transition temperature, T_g, has to be as large as possible. A difference between these values larger than 100 ^{o}C would indicate that no crystallization is expected to occur during the fiber drawing, thus increasing the probability of drawing a fiber with good optical quality including minimal scattering losses from microcrystallites [24,38]. The glasses should also exhibit similar thermal properties (viscosity/temperature response) as well as minimum mismatch in their coefficient of thermal expansion (CTE) [39,40], as large CTE mismatch can lead to the fracture of the preform and/or the fiber. Finally, for the light to be guided within the core, the refractive index of the core glass needs to be larger than that of the cladding glass [41].

In this study, the compositions of the glasses used as the core and the cladding of the fiber are the following: $97.25*(0.50P_2O_5-0.40SrO-0.10Na_2O)-2.5ZnO-0.25Er_2O_3$ and $98.25*(0.50P_2O_5-0.40SrO-0.10Na_2O)-1.75ZnO$ (in mol%), respectively. These compositions were chosen based on their good combination of optical and biological properties reported in

previous studies [12,33]. The glass used as the core was quenched into a solid rod, while the glass used as the cladding was prepared in a tube shape using the rotational casting technique (Fig. 2). No bubbles or crystals could be observed in the glasses.
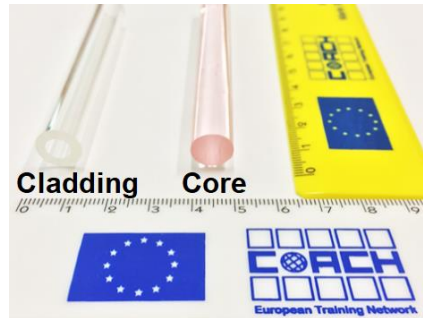

Fig. 2. Picture of the glasses used as the core and cladding of the fiber. The pink coloration of the core rod is due to the Er_2O_3 doping.

As shown in Table 1, the glasses possess similar thermal properties and so similar drawing temperature. Moreover, both glasses possess a ΔT larger than 100 °C, thus indicating that they are stable against crystallization and so suitable candidates for crystal-free fiber drawing.

Table 1

Thermal properties of the core and cladding glasses as evaluated through the DSC analysis.

Glass label	T_g ± 3 °C	T_x ± 3 °C	T_p ± 3 °C	$\Delta T = T_x - T_g$ ± 6 °C
Core	431	611	665	180
Cladding	427	615	669	188

As shown in Fig. 3, the glass used as the core of the fiber displays higher refractive index values at all the wavelengths than the glass used as the cladding. The larger refractive index

of the core glass compared to that of the cladding glass is probably due to an increase in the electron density induced by the Er^{3+} ions and the higher concentration of ZnO [42,43]. The refractive index difference between the core and the cladding at 1533 nm allows drawing a fiber with an expected numerical aperture (*NA*) of 0.09.
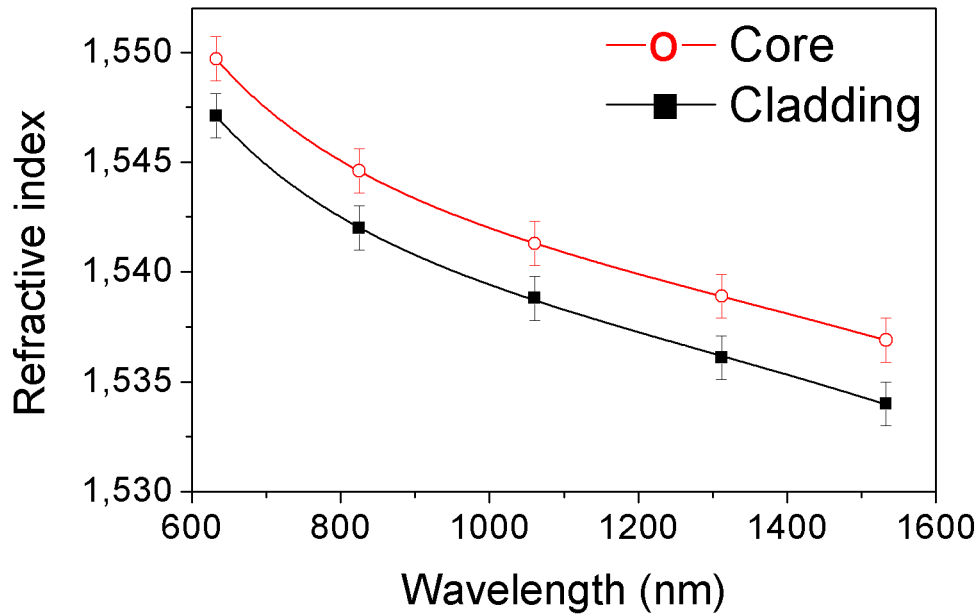

Fig. 3. Refractive index values of the core and cladding glasses measured at 5 different wavelengths and fitted with the Sellmeier's formula. The filled squares represent the experimental data, while the continuous lines are the fitting curves.

The core/cladding preform, manufactured through the rod-in-tube technique, was drawn into a multi-mode optical fiber with core/cladding diameters of around 47/119 μm. As shown in Fig. 4a, the displacement of the center of the core relative to the center of the cladding (core eccentricity) was less than 1 μm, assessing the good control during the fabrication process. No significant defects at the core/cladding interface can be observed. The near-field image of the optical fiber (Fig. 4b), acquired using a laser diode source operating at 1300 nm, clearly shows the confinement of the light in the core.
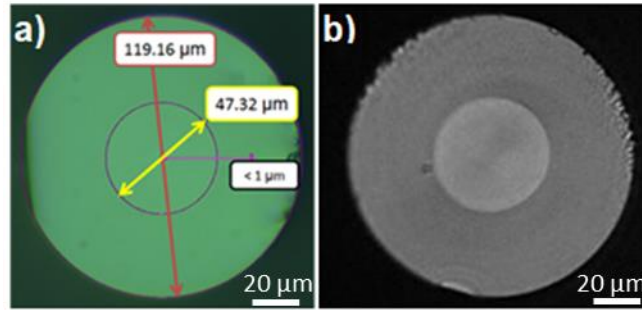
Fig. 4. Optical microscope (a) and near-field (b) images of the fiber cross-section taken with a white light source and a laser diode at 1300 nm, respectively. Both images were captured at 50X magnification.

The optical loss of the fiber at 1300 nm, evaluated by the cut-back method, was equal to (2.0 ± 0.2) dB/m, which is similar to the ones reported for other phosphate glass optical fibers [24]. Thus, based on the low attenuation loss and on the strong light confinement within the core, the fabricated optical fiber seems to be a promising material for the development of bioactive optical fiber sensors.

To monitor the reaction of the newly developed fiber when immersed in SBF through the measurement of the changes in the optical properties of the fiber core, the fiber diameter was reduced to ~75 μm using phosphoric acid (H_3PO_4, 1M) due to its well-known ability to dissolve phosphate glasses [44]. This fiber is labeled as etched fiber. Fig. 5 shows the SEM images taken at the surface and at the cross-section of the as-drawn fiber (a, b) and of a fiber etched in H_3PO_4 for 5 h. The diameter of the fiber in contact with the medium experienced a reduction of ~46 μm, corresponding to an etching rate of ~10 μm/h. Within the accuracy of the measurements (±1.5 mol%), the composition of the fiber after immersion in H_3PO_4 remained unchanged, thus indicating that the dissolution of the glass fiber in phosphoric acid was congruent.
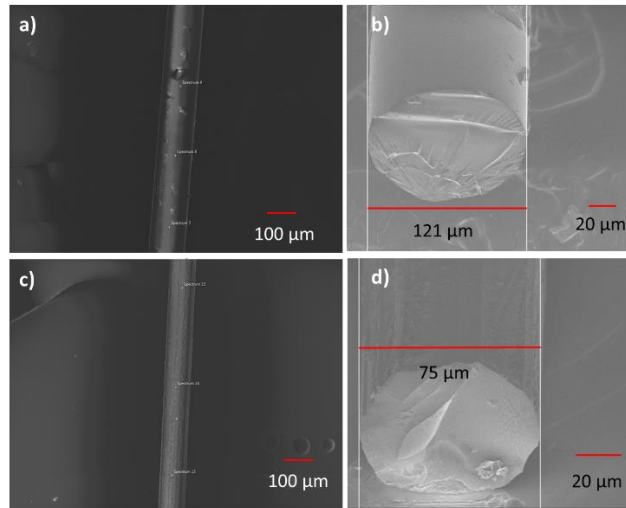
Fig. 5. SEM images taken at the surface and at the cross-section of the as-drawn fiber (a, b) and of the fiber after 5 h in H$_3$PO$_4$ (c, d).

As a proof of concept, the changes in the fiber transmission and emission properties were first measured upon immersion in phosphoric acid. The transmission and emission spectra, as well as their respective normalized Area Under Curve (AUC), are shown in Fig. 6a-c.
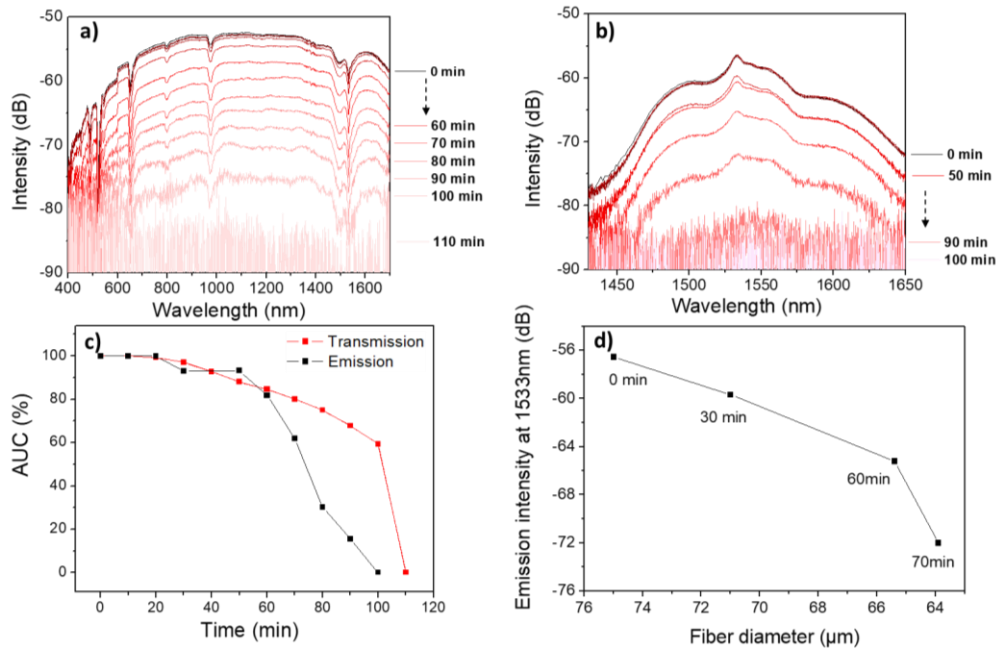
Fig. 6. Transmission (a) and emission (b) spectra of the optical fiber as a function of the immersion time in phosphoric acid solution. Normalized Area Under Curve (AUC) of the transmission and emission spectra (c). Fiber emission intensity at 1533 nm as a function of the fiber diameter upon immersion in phosphoric acid (d).

Upon immersion in phosphoric acid solution, the intensity of the fiber transmission and emission decreased. While light could still be transmitted through the fiber up to 100 min in phosphoric acid, the emission spectrum started to be noisy after only 70 min. The reason for the decrease in the fiber transmission is complex and probably due to the combination of different factors, such as: an increasing interaction of the evanescent field of the multimode fiber with the acid when reducing the cladding diameter; the increase in the roughness of the external surface of the fiber caused by the corrosion by the acid. In addition, in the case of the emission spectra, the stronger reduction observed might be due to water reabsorption caused by the diffusion of OH$^-$ hydroxyl groups in the glass, which are known to be serious quenchers of the Er^{3+} ions luminescence [45]. Nonetheless, we clearly show that it is possible to track the dissolution of the fiber over time through the changes in the optical properties of

the fiber. Therefore, the same experiment was repeated using SBF as the medium. The fiber was etched for 5 h in phosphoric acid to reduce the cladding diameter and then immersed in SBF for up to 28 days. Fig. 7 depicts the emission spectra and the AUC of the fiber collected at different time points.
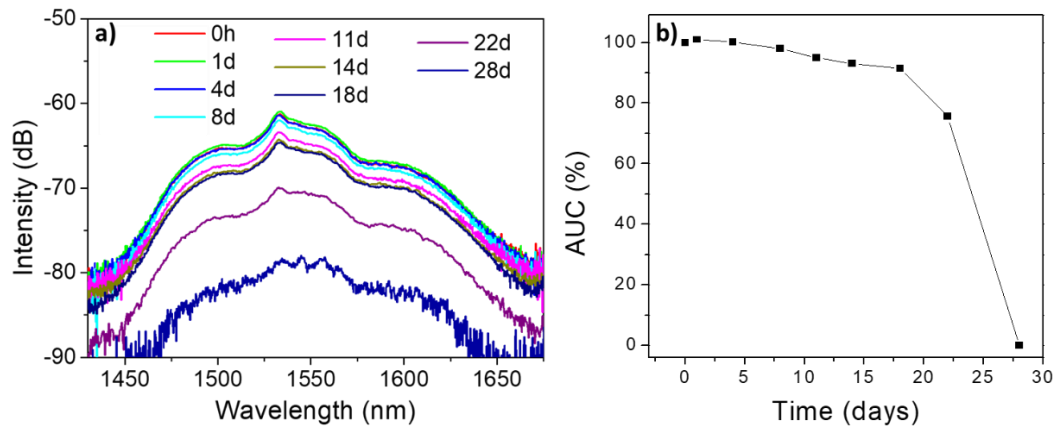

Fig. 7. Emission spectra (a) and normalized AUC (b) of the optical fiber as a function of the immersion time in SBF solution at room temperature.

Similarly to what was observed using the phosphoric acid as the dissolution medium, the fiber emission intensity progressively dropped upon immersion in SBF. Also in this case, the decrease in the intensity of the emission can be attributed to the reduction of the fiber diameter and also to the increase in the surface roughness, as evaluated through the SEM analysis. According to the SEM images of the fiber cross-section reported in Fig. 8, the diameter of the fiber after 28 days in SBF is reduced from ~72 to ~48 µm, confirming the dissolution of the fiber in SBF with a rate of ~ 0.03 µm/h.
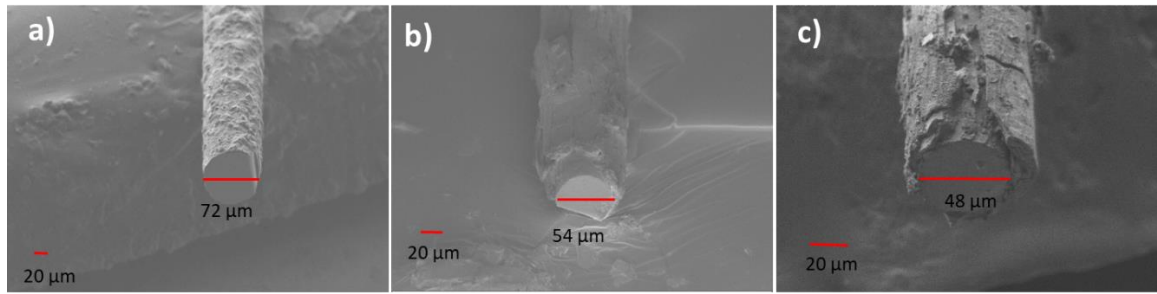
Figure 8. SEM images taken at the cross-section of the fiber immersed in SBF solution for 1 day (a), 2 days (b) and 28 days at room temperature (RT) (c).

Additionally, it is worthwhile noting that the surface of the fiber became rough just after 2 days in SBF due to the precipitation of a layer at the surface of the fiber, the thickness of which increased up to 7 µm after 28 days in SBF. The composition of the fiber surface was analyzed using EDS and the data are listed in Table 2.

Table 2

Compositional analysis of the optical fiber surface after 28 days of immersion in SBF solution.

Element (%at) (±1 %at)	O	Na	Mg	P	Cl	K	Ca	Zn	Sr
Theoretical composition of the cladding glass	65	4	0	22	0	0	0	0.4	9
After 2 days in SBF at RT	47	4	0.5	33	3	Traces	1	0.5	11
After 4 days in SBF at RT	50	6	1	29	2	1	1	Traces	10
After 28 days in SBF at RT	61	5	2	12	10	1	9	Traces	Traces
After 28 days in SBF at 37 °C	62	3	2	15	5	Traces	12	Traces	1

Elements from the SBF solution such as Ca, Mg, K and Cl were detected at the surface of the fiber. Additionally, traces of Zn and Sr were also found as well as a high amount of Ca, which is a clear indication of the formation of a Ca/P reactive layer. As previously reported

for a similar glass composition [10], the dissolution of the glass associated with the release of P in high concentration induces supersaturation of the SBF and so the precipitation of a dicalcium phosphate dehydrate (DCPD) reactive layer, where the Ca can be partially substituted by Sr and/or Mg, as confirmed here by the (Ca+Mg+Sr)/P ratio which is ~1.

The presence of the reactive layer at the surface of the fiber was also confirmed using Raman spectroscopy. The Raman spectrum of the etched fiber, presented in Fig. 9, shows the typical bands corresponding to the structure of a metaphosphate glass. A complete analysis of the Raman spectrum can be found in [33]. The broad band from 200 to 400 cm^{-1} is ascribed to the P–O bond bending mode of the Q^2 groups [46].
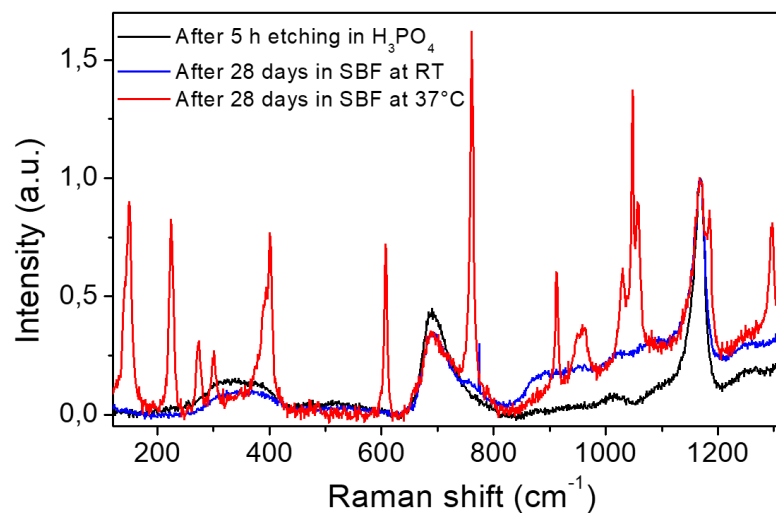

Fig. 9. Normalized Raman spectra of the phosphate fiber prior to and after immersion in SBF solution.

The immersion in SBF for 28 days leads to a slight decrease in the intensity of the bands at 300-400 cm^{-1} and at 700 cm^{-1} and also to an increase in intensity of the bands in the 800-1100 cm^{-1} region. The Raman spectrum of the fiber immersed in SBF for the same time interval but at 37 °C, which corresponds to the normal body temperature, is also shown. The spectrum shows sharp peaks which can be related to the formation of the reactive layer, in accordance

with the EDS/SEM analysis. However, while EDS/SEM analysis only provides information on the (Ca+Mg+Sr)/P ratio, the Raman spectrum gives insight on the vibrational modes involved. As expected from [31], two vibration bands, corresponding to the DCPD crystal structure, appeared at 957 (ν_1 PO$_4$) and 1057 (ν_3 PO$_4$) cm^{-1}. Nevertheless, the position and number of the vibration modes do not solely correspond to the DCPD structure. A thorough investigation of the Raman spectrum highlights the presence of peaks at 402 (ν_2 PO$_4$), 608 (ν_4 PO$_4$), 910 (P-OH), 960 (ν_1 PO$_4$), 1032 and 1048 (ν_3 PO$_4$) cm^{-1} which belong to the typical vibration bands of an octacalcium phosphate (OCP) crystal [47]. This indicates that the layer formed is most certainly a combination of the DCPD and OCP crystal structures. The only peak that could not be assigned to any calcium crystal is located at 762 cm^{-1}. This peak can be related to the asymmetric stretching vibration of the P-O-P bonds in ultraphosphate glasses, in agreement with [48]. Such surface depletion in alkaline and alkaline-earth cations in phosphate glasses immersed in aqueous solutions was reported in a previous study [49]. As shown in Fig. 8d, the reactive layer precipitated at the surface of the fiber upon immersion in SBF solution at 37 °C revealed to be thicker (~19 µm) than the one detected on the fiber immersed at room temperature (dissolution of the fiber with a rate of ~ 0.04 µm/h). Moreover, as compared to the fiber immersed at room temperature, a higher Ca concentration was found at the surface of the fiber immersed in SBF at 37 °C, thus clearly showing that the formation of the hydroxyl-apatite layer can be accelerated when the temperature is increased to 37 °C.

Finally, the integration of the phosphate optical fiber with a commercial optical fiber was also investigated. The phosphate fiber was cleaved and then fusion spliced with a commercial single-mode silica fiber with core/cladding dimensions of 7/125 µm. A picture of one of the splicing tests is shown in Fig. 10.
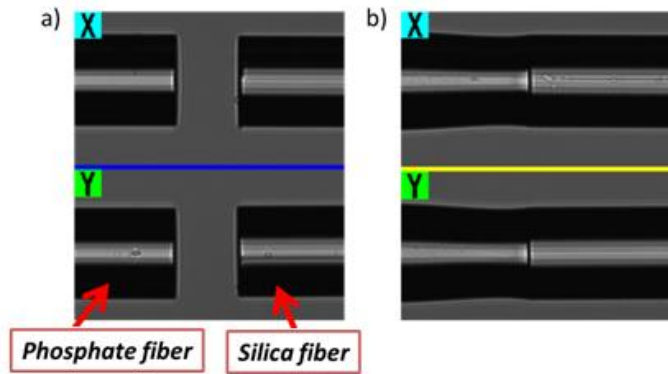
Fig. 10. Pictures taken at the end-faces of silica and phosphate optical fibers (a) before and (b) after the splicing.

The splicing was particularly challenging due to differences in geometry, composition, thermal and mechanical properties of the silica and phosphate fibers. Nonetheless, successful splice of the two fibers with good mechanical robustness was obtained as illustrated in Figure 11. A radius of curvature of 2.5 cm before breaking the fiber was achieved.
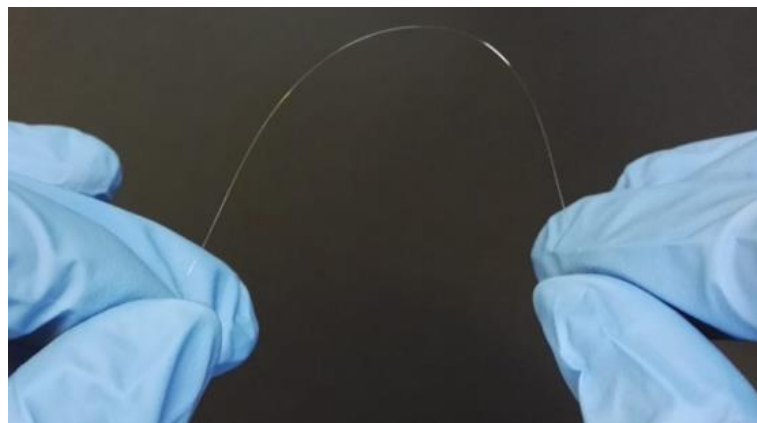

Fig. 11. Durable and mechanically robust fusion spliced joint between phosphate and silica fibers.

In order to create a continuous path of light along the spliced optical fibers, the light should not be scattered or reflected back by the splice region, and the insertion losses should be kept

as minimum. Various splicing tests were performed using ~10 cm-long segments of phosphate and silica fibers. The fusion splice insertion losses were obtained by measuring the difference between the input and the output signals. An average insertion loss of (0.3 ± 0.1) dB was obtained, thus confirming that the phosphate optical fiber sensor can be successfully spliced with commercial silica fibers, broadening its field of applications.

5. Conclusions

In this paper, Er^{3+}-doped core and un-doped cladding preforms were successfully drawn into an optically active core and bioactive cladding fiber. For the first time, the biological and optical responses of a bioactive Er^{3+}-doped optical fiber when immersed in aqueous media were measured. The changes in the optical fiber diameter followed a linear etching rate of ~10 μm/h when using H_3PO_4. A decrease in the emission spectrum intensity upon immersion in SBF solution was also reported and related to the progressive decrease in the fiber diameter. Based on the EDS/SEM and Raman analyses, a reactive layer started to precipitate at the surface of the fiber just after 2 days in SBF. The reactive layer is composed of both dicalcium phosphate dehydrate and octacalcium phosphate, both being appropriate substrates for cells adhesion and proliferation, thus confirming the bioactivity of the fiber. A faster reaction rate was observed when the temperature of SBF was increased to 37 °C.

Overall, with this study, it is clearly shown that it is possible to track the degradation and bioactivity reaction of an optically active and bioactive fiber when immersed in aqueous media through the changes in its spectroscopic properties. These investigations pave the way toward the use of optical fibers for the development of new biophotonic sensing probes, which could monitor "in situ" the dissolution and bioactivity behavior of the fiber inside the human body in the prospect of developing innovative biosensors for therapy monitoring. Furthermore, recent medical procedures such as Photo Dynamic Therapy (PDT), which

require the delivery of light in deep tissue areas of the body, will benefit from biocompatible devices such as bioactive optical fibers, which can lead to soft tissue regeneration and thus their surgical removal would not be needed.

6. Acknowledgments

References

1. Hench LL, Splinter RJ, Allen WC, Greenlee TK. Bonding mechanisms at the interface of ceramic prosthetic materials. J. Biomed. Mater. Res. 1971;5(6):117–41. https://doi.org/10.1002/jbm.820050611 [online article]

2. Fagerlund S, Massera J, Hupa M, Hupa L. T-T-T behaviour of bioactive glasses 1-98 and 13-93. J. Eur. Ceram. Soc. 2012;32(11):2731–8. https://doi.org/10.1016/j.jeurceramsoc.2011.10.040 [online article]

3. Pirhonen E, Niiranen H, Niemelä T, Brink M, Törmälä P. Manufacturing, mechanical characterization, and in vitro performance of bioactive glass 13-93 fibers. J. Biomed. Mater. Res. - Part B Appl. Biomater. 2006;77(2):227–33.

https://doi.org/10.1002/jbm.b.30429 [online article]

4. Groh D, Döhler F, Brauer DS. Bioactive glasses with improved processing. Part 1. Thermal properties, ion release and apatite formation. Acta Biomater. 2014;10(10):4465–73. https://doi.org/10.1016/j.actbio.2014.05.019 [online article]

5. Baino F, Vitale-Brovarone C. Three-dimensional glass-derived scaffolds for bone tissue engineering: current trends and forecasts for the future. J. Biomed. Mater. Res - Part A. 2011;97:514–35. https://doi.org/10.1002/jbm.a.33072 [online article]

6. Montazerian M, Zanotto ED, A guided walk through Larry Hench's monumental discoveries. Journal of Materials Science.2017;52 (15):8695-8732 https://doi.org/10.1007/s10853-017-0804-4 [online article]

7. Uo M, Mizuno M, Kuboki Y, Makishima A, Watari F. Properties and cytotoxicity of water soluble Na_2O–CaO–P_2O_5 glasses. Biomaterials. 1998;19(24):2277–84. https://doi.org/10.1016/S0142-9612(98)00136-7 [online article]

8. Suzuya K, Price DL, Loong CK, Kohara S. Structure of magnesium phosphate glasses. J. Phys Chem Solids. 1999;60(8):1457–60. https://doi.org/10.1016/S0022-3697(99)00140-7 [online article]

9. Ahmed I, Lewis M, Olsen I, Knowles JC. Phosphate glasses for tissue engineering: part 1. Processing and characterisation of a ternary-based P_2O_5–CaO–Na_2O glass system. Biomaterials.2004;25(3):491–9. https://doi.org/10.1016/S0142-9612(03)00546-5 [online article]

10. Massera J, Petit L, Cardinal T, Videau JJ, Hupa M, Hupa L. Thermal properties and surface reactivity in simulated body fluid of new strontium ion-containing phosphate glasses. J. Mater. Sci. Mater. Med. 2013;24(6):1407–16. https://doi.org/10.1007/s10856-013-4910-9 [online article]

11. Sharmin N, Hasan MS, Parsons AJ, Furniss D, Scotchford CA, Ahmed I, et al. Effect

of boron addition on the thermal, degradation, and cytocompatibility properties of phosphate-based glasses. Biomed. Res. Int. 2013;902427. http://dx.doi.org/10.1155/2013/902427 [online article]

12. Massera J, Kokkari A, Narhi T HL. The influence of SrO and CaO in silicate and phosphate bioactive glasses on human gingival fibroblasts. J. Mater. Sci. Mater. Med. 2015;26(6):196. https://doi.org/10.1007/s10856-015-5528-x [online article]

13. Bunker BC, Arnold GW, Wilder JA. Phosphate glass dissolution in aqueous solutions. J. Non Cryst. Solids. 1984;64(3):291–316. https://doi.org/10.1016/0022-3093(84)90184-4 [online article]

14. Knowles JC. Phosphate based glasses for biomedical applications. J. Mater. Chem. 2003;13(10):2395–401. https://doi.org/10.1039/b307119g [online article]

15. Clement J, Manero JM, Planell JA, Avila G, Martinez S. Analysis of the structural changes of a phosphate glass during its dissolution in simulated body fluid. J. Mater. Sci. Mater. Med. 1999;10(12):729–32. https://doi.org/10.1023/A:1008927222081 [online article]

16. Campbell JH, Suratwala TI. Nd-doped phosphate glasses for high-energy/high-peak-power lasers. J. Non Cryst. Solids. 2000;263:318–41. https://doi.org/10.1016/S0022-3093(99)00645-6 [online article]

17. Jiang S, Myers MJ, Rhonehouse DL, Hamlin SJ, Myers JD, Griebner U, et al. Ytterbium-doped phosphate laser glasses. 1997;2986:10–5. https://doi.org/10.1117/12.269990 [online article]

18. Gapontsev VP, Matitsin SM, Isineev AA, Kravchenko VB. Erbium glass lasers and their applications. Opt. Laser Technol. 1982;14(4):189–96. https://doi.org/10.1016/0030-3992(82)90095-0 [online article]

19. Jiang S, Myers M, Peyghambarian N. Er^{3+} doped phosphate glasses and lasers. J. Non

Cryst. Solids. 1998;239(1–3):143–8. https://doi.org/10.1016/S0022-3093(98)00757-1 [online article]

20. Pugliese D, Boetti NG, Lousteau J, Ceci-Ginistrelli E, Bertone E, Geobaldo F, et al. Concentration quenching in an Er-doped phosphate glass for compact optical lasers and amplifiers. J. Alloys Compd. 2016;657:678–83. https://doi.org/10.1016/j.jallcom.2015.10.126 [online article]

21. Boetti NG, Scarpignato GC, Lousteau J, Pugliese D, Bastard L, Broquin J-E, et al. High concentration Yb-Er co-doped phosphate glass for optical fiber amplification. J. Opt. 2015;17(6):065705. https://doi.org/10.1088/2040-8978/17/6/065705 [online article]

22. Vitale-Brovarone C, Novajra G, Milanese D, Lousteau J, Knowles JC. Novel phosphate glasses with different amounts of TiO_2 for biomedical applications: dissolution tests and proof of concept of fibre drawing. Mater. Sci. Eng. C. 2011;31(2):434–42. https://doi.org/10.1016/j.msec.2010.11.001 [online article]

23. Sharmin N, Parsons AJ, Rudd CD, Ahmed I. Effect of boron oxide addition on fibre drawing, mechanical properties and dissolution behaviour of phosphate-based glass fibres with fixed 40, 45 and 50 mol% P_2O_5. J. Biomater. Appl. S. 2014;29(5):639–53. https://doi.org/10.1177/0885328214539824 [online article]

24. Ceci-Ginistrelli E, Pugliese D, Boetti NG, Novajra G, Ambrosone A, Lousteau J, et al. Novel biocompatible and resorbable UV-transparent phosphate glass based optical fiber. Opt. Mater. Express. 2016;6(6):2040–51. https://doi.org/10.1364/OME.6.002040 [online article]

25. Novajra G, Lousteau J, Milanese D, Vitale-Brovarone C. Resorbable hollow phosphate glass fibres as controlled release systems for biomedical applications. Mater. Lett. 2013;99:125–7. https://doi.org/10.1016/j.matlet.2013.02.076 [online article]

26. Vitale-Brovarone C, Novajra G, Lousteau J, Milanese D, Raimondo S, Fornaro M. Phosphate glass fibres and their role in neuronal polarization and axonal growth direction. Acta Biomater. 2012;8(3):1125–36. https://doi.org/10.1016/j.actbio.2011.11.018 [online article]

27. Jiang S, Luo T, Hwang BC, Smekatala F, Seneschal K, Lucas J, et al. Er^{3+}-doped phosphate glasses for fiber amplifiers with high gain per unit length. J. Non Cryst. Solids. 2000;263:364–8. https://doi.org/10.1016/S0022-3093(99)00646-8 [online article]

28. Hofmann P, Voigtlander C, Nolte S, Peyghambarian N, Schulzgen A. 550-mW output power from a narrow linewidth all-phosphate fiber laser. J. Light Technol. 2013;31(5):756–60. https://doi.org.10.1109/JLT.2012.2233392 [online article]

29. Hwang BC, Jiang S, Luo T, Seneschal K, Sorbello G, Morrell M, et al. Performance of high-concentration Er^{3+}-doped phosphate fiber amplifiers. IEEE Photonics Technol. Lett. 2001;13(3):197–9. https://doi.org.10.1109/68.914319 [online article]

30. Massera J, Shpotyuk Y, Sabatier F, Jouan T, Boussard-Plédel C, Roiland C, et al. Processing and characterization of novel borophosphate glasses and fibers for medical applications. J. Non Cryst. Solids. 2015;425:52–60. https://doi.org/10.1016/j.jnoncrysol.2015.05.028 [online article]

31. Keiser G, Xiong F, Cui Y, Shum PP. Review of diverse optical fibers used in biomedical research and clinical practice. J. Biomed. Opt. 2014;19(8):080902. https://doi.org/10.1117/1.JBO.19.8.080902 [online article]

32. Massera J, Ahmed I, Petit L, Aallos V, Hupa L. Phosphate-based glass fiber vs. bulk glass: Change in fiber optical response to probe in vitro glass reactivity. Mater. Sci. Eng. C. 2014;37(1):251–7. https://doi.org/10.1016/j.msec.2014.01.021 [online article]

33. Lopez-Iscoa P, Petit L, Massera J, Janner D, Boetti NG, Pugliese D, et al. Effect of the

addition of Al_2O_3, TiO_2 and ZnO on the thermal, structural and luminescence properties of Er^{3+}-doped phosphate glasses. J. Non Cryst. Solids. 2017;460:161–8. https://doi.org/10.1016/j.jnoncrysol.2017.01.030 [online article]

34.   Dash A, Kumar-Pal S, Banerjee I, Chakraborty S. Rare-earth-doped SiO_2-CaF_2 glass ceramic nano-particle with upconversion properties. Int. J. Appl. Sci. Tech. 2018;15(1):223-231. https://doi.org/10.1111/ijac.12769 [online article]

35.   Anne ML, Keirsse J, Nazabal V, Hyodo K, Inoue S, Boussard-Pledel C, Lhermite H, Charrier J, Yanakata K, Loreal O, Le Person J, Colas F, Compère C, Bureau B, Chalcogenide Glass Optical Waveguides for Infrared Biosensing, Sensors, 2009;9: 7398-7411. https://doi.org/10.3390/s90907398 [online article]

36.   Tatian B. Fitting refractive-index data with the Sellmeier dispersion formula. Appl. Opt. 1984;23:4477–4485. https://doi.org/10.1364/AO.23.004477 [online article]

37.   Kokubo T, Kushitani H, Sakka S, Kitsugi T, Yamamuro T. Solutions able to reproducein vivo surface-structure changes in bioactive glass-ceramic A-W3. J. Biomed. Mater. Res. 1990;24(6):721–34. https://doi.org/10.1002/jbm.820240607 [online article]

38.   Mura E, Lousteau J, Milanese D, Abrate S, Sglavo VM. Phosphate glasses for optical fibers: Synthesis, characterization and mechanical properties. J. Non Cryst. Solids. 2013;362(1):147–51. https://doi.org/10.1016/j.jnoncrysol.2012.11.029 [online article]

39.   Ceci-Ginistrelli E, Smith C, Pugliese D, Lousteau J, Boetti NG, Clarkson WA, et al. Nd-doped phosphate glass cane laser: from materials fabrication to power scaling tests. J. Alloys Comp. 2017;722:599–605. https://doi.org/10.1016/j.jallcom.2017.06.159 [online article]

40.   Martin RA, Knight JC. Silica-clad neodymium-doped lanthanum phosphate fibers and fiber lasers. IEEE Photonics Technol Lett. 2006;18(4):574–6.

https://doi.org/10.1109/LPT.2005.863999 [online article]

41. Carlie N, Petit L. Engineering of glasses for advanced optical fiber applications. J. Eng. Fibers Fabr. 2009;4:21–29. https://doi.org/10.1177/155892500900400410 [online article]

42. Said Mahraz ZA, Sahar MR, Ghoshal SK, Reza Dousti M. Concentration dependent luminescence quenching of Er^{3+}-doped zinc boro-tellurite glass. J. Lumin. 2013;144:139–45. https://doi.org/10.1016/j.jlumin.2013.06.050 [online article]

43. Stambouli W, Elhouichet H, Ferid M. Study of thermal, structural and optical properties of tellurite glass with different TiO_2 composition. J. Mol. Struct. 2012;1028:39–43. https://doi.org/10.1016/j.molstruc.2012.06.027 [online article]

44. Colquhoun R, Tanner KE. Mechanical behaviour of degradable phosphate glass fibres and composites - A review. Biomed Mater. 2015;11:014105. https://doi.org.10.1088/1748-6041/11/1/014105 [online article]

45. Yan Y, Faber AJ, de Waal H. Luminescence quenching by OH groups in highly Er-doped phosphate glasses. J. Non Cryst. Solids. 1995;181(3):283–90. https://doi.org/10.1016/S0022-3093(94)00528-1 [online article]

46. Hockicko P, Kudelcik J, Munoz F, Munoz-Senovilla L. Structural and Electrical Properties of $LiPO_3$ Glasses. Adv. Electr. Electron. Eng. 2015;13:198–205. https://doi.org.10.15598/aeee.v13i2.1250 [online article]

47. Rey C, Marsan O, Combes C, Drouet C, Grossin D, Sarda S. Characterization of Calcium Phosphates Using Vibrational Spectroscopies. Advances in Calcium Phosphate Biomaterials. 2014;1:229–66 [online article]

48. Hussin R, Ahmad Salim M, Alias NS, Abdullah MS, Abdullah S, Ahmad Fuzi SA, et al. Vibrational Studies of Calcium Magnesium Ultraphosphate Glasses. J. Fundam. Appl. Sci. 2009;5:41–53. https://doi.org/10.11113/mjfas.v5n1.286 [online article]

49. Naruphontjirakul P, Greasley SL, Chen S, Porter AE, Jones JR. Monodispersed strontium containing bioactive glass nanoparticles and MC3T3-E1 cellular response. Biomedical Glasses. 2016;2:72–81. https://doi.org/10.1515/bglass-2016-0009 [online article]